Isotope Signs (^{234}U/^{238}U, ^{2}H, ^{18}O) of Groundwater: An Investigation of the Existence of Paleo-Permafrost in European Russia (Pre-Volga Region)

Evgeny Yakovlev [1,*], Igor Tokarev [2], Sergey Zykov [1], Stanislav Iglovsky [1] and Nikolay Ivanchenko [1,3]

[1] N. Laverov Federal Center for Integrated Arctic Research of UB RAS, 163000 Arkhangelsk, Russia; abs2417@yandex.ru (S.Z.); iglovskys@mail.ru (S.I.)

[2] Research Park, St. Petersburg State University, 198504 St. Petersburg, Russia; tokarevigor@gmail.com

[3] Northern (Arctic) Federal University, 163002 Arkhangelsk, Russia; ivanchenkonl@mail.ru

[*] Correspondence: evgeny.yakovlev@fciarctic.ru; Tel.: +7-818-221-15-71

Abstract: The isotopic (^{234}U/^{238}U, ^{2}H, ^{18}O) and chemical composition of groundwater on the right bank of the Volga River along the middle reach (European Russia) was studied down to a depth of 400 m. These data allow diagnosis of the presence of a three-component mixture. The first component is modern/young fresh recharge water of the Holocene age. It has the isotopic composition of water δ^{18}O $\rightarrow$ -12.9 ‰ and δ^{2}H $\rightarrow$ -90 ‰, close to modern precipitations, and the equilibrium isotopic composition of uranium ^{234}U/^{238}U $\rightarrow$ 1 (by activity). The second component is slightly salted water of the late or postglacial period with δ^{18}O $\rightarrow$ -17.0 ‰ and δ^{2}H $\rightarrow$ -119 ‰, and a small excess of uranium-234 ^{234}U/^{238}U $\approx$ 4. The third component is meltwater formed as result of permafrost thawing. It is brackish water with δ^{18}O $\approx$ -15.0 ‰ and δ^{2}H $\approx$ -110 ‰, and a maximum excess of uranium-234 ^{234}U/^{238}U $\approx$ 15.7. The salinity of this water is associated with an increase of the SO$_4^{2-}$, Ca^{2+} and Na^{+} content, and this may be due to the presence of gypsum in water-bearing sediments, because the solubility of sulfates increases at near-zero temperature. We explain the huge excess of uranium-234 by its accumulation in the mineral lattice during the glacial age and quick leaching after thawing of permafrost.

Keywords: groundwater; stable isotopes; uranium-234; permafrost; Pre-Volga

1. Introduction

During the Weichselian glaciation (about 110–12 ka ago, the below mentioned Valdai cryochron according to the Russian notation), continental glaciation occurred repeatedly and its characteristics have been studied quite well for the East European Plain [1–26].

Geomorphological, textural, pedological, faunistic, micropaleontological, pollen, and geochemical signs indicate that a dry, cold and windy climate of the Arctic steppes with sparse cold-tolerant vegetation was prevalent in the periglacial area [27–35]. Cold conditions are marked by the wide distribution of loess, relics of the aeolian dune relief, and the asymmetric structure of river valleys [36–39]. In the Valdai cryochron, most of the East European Plain was an area of continuous permafrost. For example, in its central part during the MIS-2 the permafrost was 200–250 m thick, and the ground temperature was about -5 °C [40]. There are no data on the degree of permafrost degradation within the warm episodes of the Valdai cryochron. However, it can be assumed that the ground ice was not completely melted due to the low vertical hydraulic permeability of the geological section, as aquicludes prevented percolation of the warm recharge water to a significant depth.

After the disappearance of permafrost in the Holocene, the soil-forming processes and chemical weathering were intensified [41,42]. The paleocryogenic microrelief was buried and levelling of the earth surface took place due to the soil flow and modern sediment accumulation [43–46]. Meltwater formed from the thawed permafrost and ice-wedges

(hereafter referred to as a glacial meltwater). In the upper part of the geological section, it should have been replaced by young recharge water with modern and/or Holocene age, but the low permeability of the clayey layers could to preserve the meltwater at depth.

It is clearly known that global climatic variations are reliably recorded using stable isotopes [47–51]. Groundwater, which formed during the cold period due to meteoric water recharge, has a depleted (light) isotopic composition of hydrogen and oxygen, i.e., very negative values of $\delta^{18}O$ and δ^2H. Cryogenic metamorphism is also possible during permafrost growth. In the frozen zone, the isotopic composition of ice could be less depleted by deuterium and oxygen-18 relative to the initial recharge water of atmospheric origin. In contrast, the residual water, which is accumulated at the base layer of the permafrost, should be more depleted by ^{18}O and ^2H relative to the initial isotope composition [52]. At the same time, the ice in permafrost (and also glacial meltwater) is desalinated, and the lost salts accumulate in the residual water. This process can lead to the formation of inversion chemical zonation in the depths below the bottom of the former permafrost [52].

The authors of this work also assume that the glacial meltwater should be marked as an anomaly in the isotopic composition of uranium $^{234}U/^{238}U > 1$ (hereafter in the activity ratio) due to the excess of uranium-234. The mechanism of equilibrium loss may be result of the very different geochemical mobility of parent uranium-238 and daughter uranium-234. Usually, ^{234}U has the oxidation state 6+, which is soluble and could be transported with water in uranyl complexes, but ^{238}U has the oxidation state 4+ and is included in the mineral lattice as non-soluble forms [53–55]. Additionally, ^{234}U is located in connection with the recoil tracks of α-particle and ^{234}Th (first daughter isotope to ^{238}U), so the diffusion coefficient of ^{234}U atoms in the mineral lattice is more than it is for ^{238}U atoms by about two orders, as we calculated. As liquid water was non-available during a significant geological time period, such as the Valdai cryochron, uranium-234 generated in minerals as the normal component of the radioactive chain ($^{234}U/^{238}U = 1$). When meltwater from the thawed permafrost appeared, then predominantly ^{234}U would be rapidly leached from the water-bearing sediments and rocks compared to ^{238}U. Therefore, the glacial meltwater (but not the next portions of the recharge water) should be marked by $^{234}U/^{238}U > 1$. For some areas in Russia, which were under periglacial conditions in the last ice age, this hypothetical mechanism received confirmation from a complex study of groundwater, including the determination of $\delta^{18}O$, δ^2H, $^{234}U/^{238}U$, Noble Gas Temperature calculation and the dating of groundwater by the helium technique [56–59]. Thus, the isotopic ratio $^{234}U/^{238}U$ can be used to diagnose the presence of glacial meltwater at the present time and to estimate the freezing depth of the geological section during the glacial period.

In this work, the Pre-Volga region (right bank of the Volga River along the middle reach) was studied, where groundwater was sampled down to a depth of 400 m for determination of the chemical and isotope composition of the water.

2. Characterization of the Studied Area

The area is a hilly plain with absolute marks of thalweg of the river valleys down to 40 and watersheds up to 230 m. The main drains are the Sviyaga and the Sura rivers (both are right tributaries of the Volga River). River valleys are usually trough- and U-shaped, while watersheds are plateau-like. Local elevation differences usually do not exceed 80–100 m. The modern climate of the Pre-Volga region is temperate continental with an average annual air temperature of +2.9 °C. The snow cover lasts 120–160 days and the depth of seasonal freezing is 1.8 m. The Yaroslavsky (MIS-2 12.2–20 ka) and Selikhovodvorsky (MIS-4 58–71 ka) cryogenic soils mark the coldest climatic stages of the Valdai cryochron in the study area (Table 1). There was no ice cover on the Pre-Volga region in this period, and only a small area on the highest watersheds was probably iced [60]. The boundary of the continuous permafrost was located far to the south of the study area (Figure 1).

Table 1. Cryogenic sediments and soils of Pre-Volga region according to the reference section in the Aleksandrovsky quarry ([61] with changes).

MIS	Stage	Age, ka	Paleo-relief forms, cryotextures	Frosty conditions
5e	Mikulino	128–117	Small wedges data	Seasonal permafrost
5d	Early Valdai Stadium 1	117–100	Plastic deformations, small pseudomorphs on wedges, etc.	Discontinuous permafrost
5c	Early Valdai Interstadial 1	100–91	Ground veins—humus tongues	Seasonal freezing and drying out
5b	Early Valdai Stadium 2	91–77	Small wedges	Discontinuous permafrost
5a	Early Valdai Interstadial 2	77–71	Soil veins—humus tongues-cosmas	Seasonal freezing and drying out
4	Early Valdai Stadium 3	71–58	Pseudomorphs on ice wedges, 0.6 m wide, 0.5 m deep, and post-cryogenic textures	Continuous and discontinuous permafrost
3	Middle Valdai interstadial 1	58–49.5	Small cracks, gleying	Deep seasonal freezing
3	Middle Valdai Stadium 1	49.5–32.0	Plastic deformations and small wedges	Discontinuous permafrost
3	Middle Valdai Interstadial 2	32.0–24.0	Wedges	Deep seasonal freezing
2	Maximum glaciation and late glacial	24.0–12.2	Large wedge-shaped structures. Dells.	Continuous permafrost, then intermittent and seasonal permafrost
1	Holocene	11.6–0		Seasonal freezing
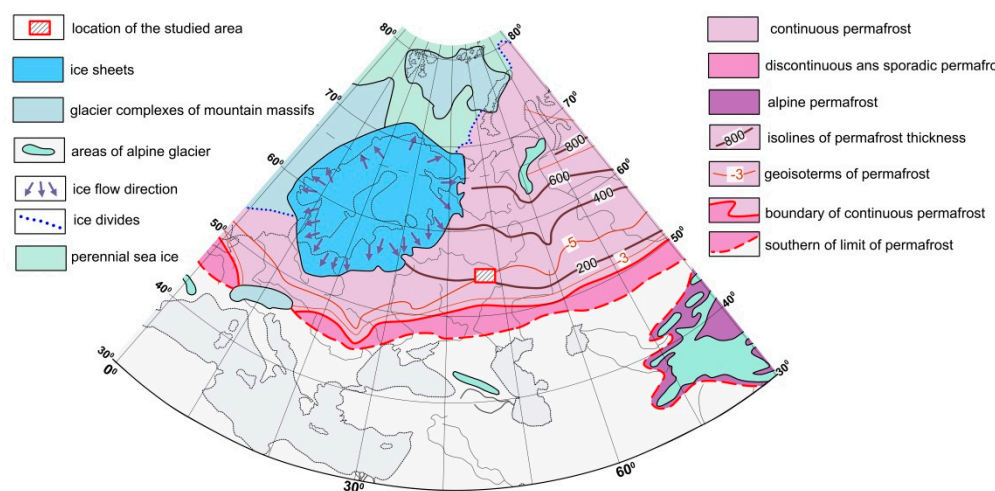
Figure 1. Glaciation and permafrost on the Eastern Europe Plain during the Last Glacial Maximum 20–18 thousand years ago ([40] with changes).

The upper part (400–600 m) of the geological section in the studied area is composed of Paleozoic, Mesozoic and Cenozoic sediments (Figure 2).

The Paleozoic-Mesozoic strata are represented by interlayering of the terrigenous-carbonate formation (mostly argillites and dolomites) with inclusions of evaporite—anhydrite, gypsum and, rarely, rock salts. The thickness of the Late Cenozoic sediments (the Neogene and the Quaternary) varies from 1 to 35 m, but the buried valleys of the paleo-rivers can sometimes reach a depth of 200 m. Excluding the alluvial sediments in the river valleys, all Quaternary facies have a clayey or loamy composition [62].
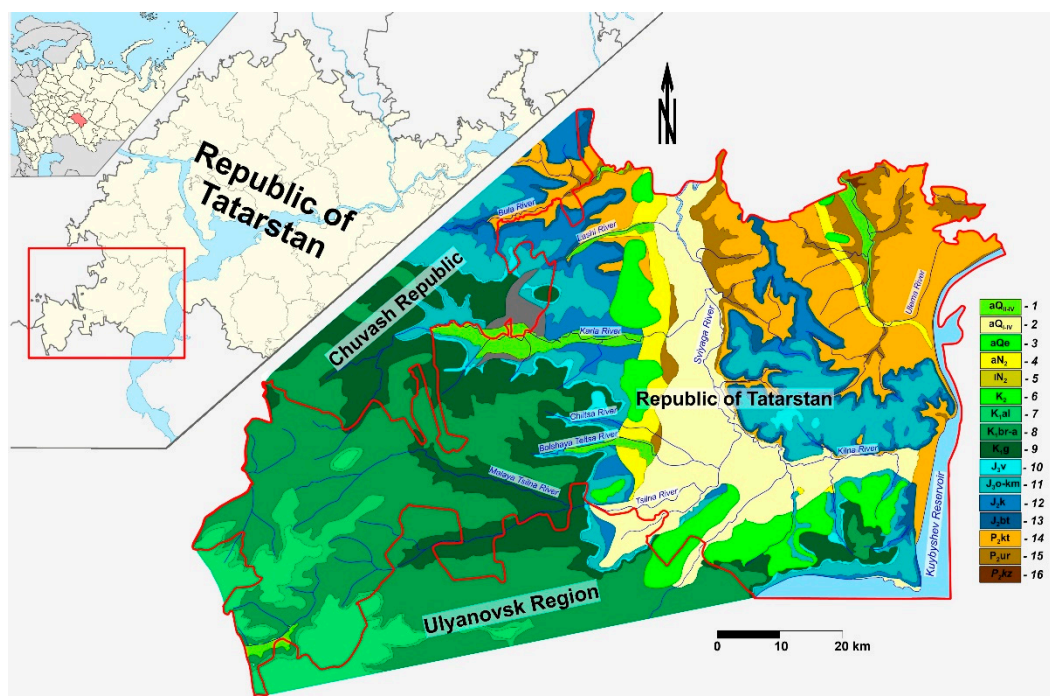
Figure 2. Hydrogeological map of the study area [63]: *1*—Medium Quaternary to modern alluvial aquifer; *2*—Lower Quaternary to modern alluvial low-yielding aquifer; *3*—Eopleistocene alluvial aquifer; *4*—Pliocene alluvial aquifer; *5*—Pliocene impermeable lacustrine aquitard; *6*—Upper Cretaceous terrigenous-carbonate low-yielding aquifer; *7*—Albian terrigenous low-yielding aquifer; *8*—Barremian-Aptian terrigenous aquiclude layer; *9*—Hauterivian terrigenous aquiclude layer; *10*—Volzhsky terrigenous aquiclude layer; *11*—Oxford-Kimmeridgian terrigenous aquiclude layer; *12*—Callovian terrigenous aquiclude layer; *13*—Bathonian terrigenous low-yielding aquifer; *14*—Kotelnikiy carbonate-terrigenous aquifer; *15*—Urzhum terrigenous-carbonate aquifer; *16*—Kazan sulfate-carbonate karstified aquifer.

All shallow aquifers (which are first from earth surface) from the alluvium (aQ_{I-IV} and N_2) to the Urzhum suite (P_2ur) have modern recharge, as is clearly seen from the ^3H content in most times. The Urzhum suite sediments are dried on the local watersheds. The total volume of freshwater in the phreatic zone of the main catchments is calculated at 11.7 km^3. Taking into account the modulus of the minimum winter 30-day river runoff for a year of 95% supply and the calculated volume of freshwater, the residence time of groundwater in the zone of the active water exchange is $\tau \approx 200$–3000 years, and on average, 1900 years.

3. Materials and Methods

In 2020 during August 15–28 on the study area 33 groundwater samples were taken from the Quaternary, Cretaceous, Jurassic and Permian aquifers at depths down to 400 m (Figure 3 and Table A1). Water samples were mainly taken from boreholes operated by submersible electric pumps, and in some cases from wells and springs.

Unstable parameters—pH, Eh (redox potential), electrical conductivity (mineralization), and temperature—were determined in the field immediately after sampling. The measurement of pH and Eh was carried out using a portable combined device, Hanna Instruments HI-9126 (Hanna Instruments, Woonsocket, USA), and the electrical conductivity and water temperature—using a conductometer, VZOR Mark-603/1 (LLC "VZOR", Moscow, Russia).
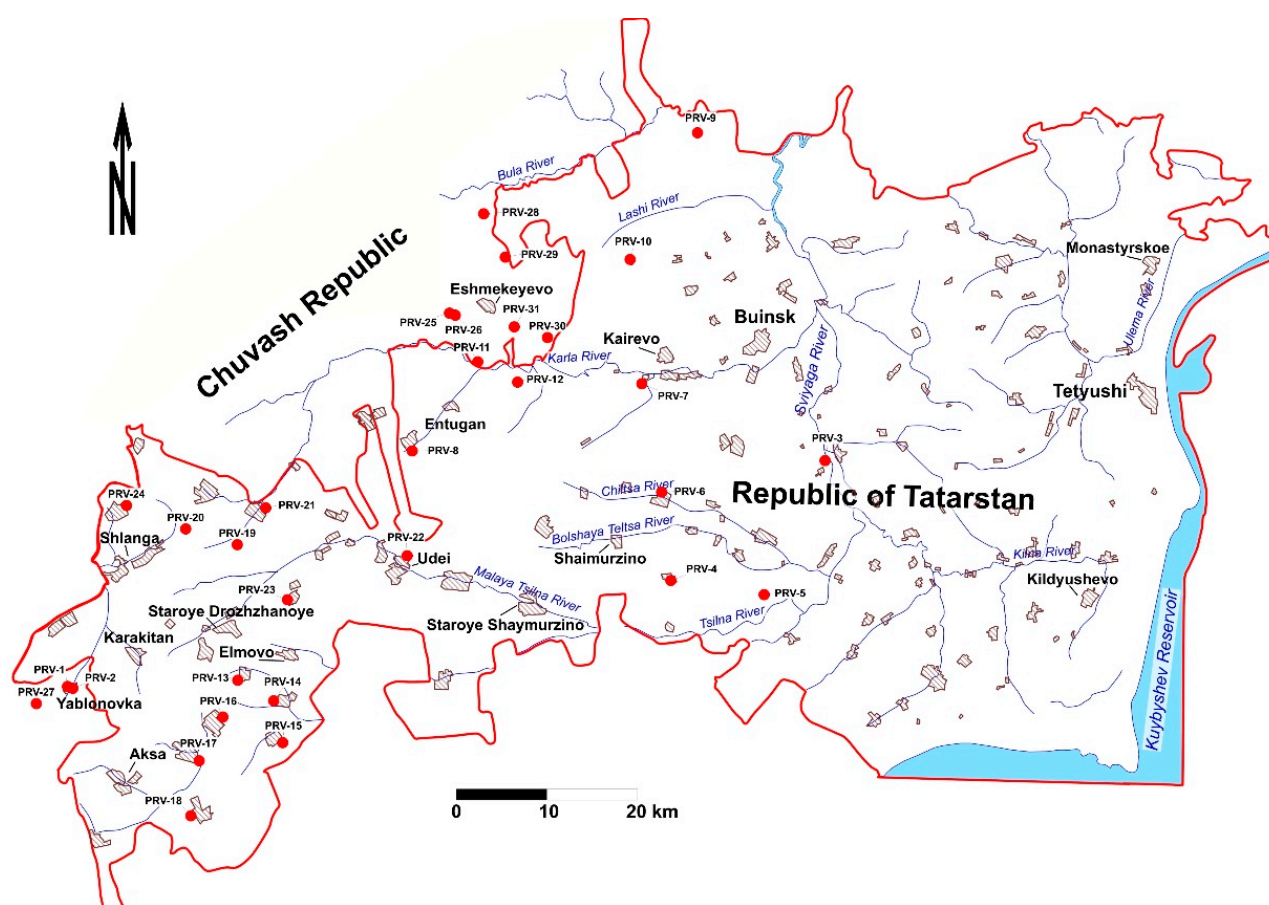
Figure 3. Location of the studied area and sampling points (red solid circles).

Water samples to determine the trace metals were taken in 50 mL plastic bottles, filtered through a membrane filter with a pore size of 0.45 μm, and acidified by high purity grade HNO_3 to pH < 2. Disposable gloves and syringes were used for each sample. The content of trace elements was measured by the atomic absorption method using a Shimadzu AA-7000 spectrometer. In 1999–2007, the chemical composition of the groundwater (major components, as a rule, and microelements in small part of samples) was studied by standard chemical techniques in 839 samples [56].

Water samples for the stable isotopes ($\delta^2 H$ and $\delta^{18}O$) were taken in plastic bottles with a volume of 10 mL without conservation. Determination of $\delta^2 H$ and $\delta^{18}O$ was carried out using a Picarro L-2120i infrared ring-down spectrometer (Picarro Inc., Santa Clara, CA, USA) in the Research park of Saint-Petersburg State University. The results were expressed in δ-notation relative to the Vienna Standard Mean Ocean Water (V-SMOW-2). The precision of the method is $\pm 0.1‰$ for $\delta^{18}O$ and $\pm 1.0‰$ for $\delta^2 H$. Standards USGS-45 and USGS-46 were used for calibration.

Preconcentration of uranium was preconcentrated from 25 L water samples under field conditions using BAU-A (charcoal) sorbent. The yield of uranium was controlled by the activity of synthetic ^{232}U isotope as tracer, which was added to the samples during collection. Radiochemical preparation included the desorption of uranium from sorbent, purification from co-precipitated radioactive elements by the extraction method using tributyl phosphate, and electrolytic deposition of uranium on polished stainless-steel discs. The measurements were performed by semiconductor alpha spectrometers Progress and Multirad-AS (from Doza, Russia) with an error of 3–7%. The quality of the measurements was checked by analyzing an OSK U7 equilibrium uranium reference sample (VIMS Institute, Moscow, Russia).

4. Results and Discussion

Generally, in the study area the vertical chemical zonation of the groundwater is as follows [56].

At depths from 0 to 100 m, mainly fresh water is contained (salinity in gram per liter and contents of chemical components in % mg-eq./L):

$$S = 0.4\text{--}1.0 \quad \frac{\begin{array}{c} HCO_3(70\text{--}96)\ NO_3(1\text{--}18) \\ Cl(1\text{--}6)\ SO_4(1\text{--}6) \end{array}}{Ca(22\text{--}69)\ Mg(7\text{--}49)\ Na(2\text{--}37)} \quad pH = 7.5\text{--}7.8.$$

In the river valleys, where discharge of the brackish deep-water occurred, the sulfate-sodium type of groundwater is formed:

$$S = 0.9\text{--}1.8 \quad \frac{\begin{array}{c} SO_4(36\text{--}63)\ HCO_3(27\text{--}52) \\ Cl(2\text{--}17) \end{array}}{Na(14\text{--}86)\ Mg(9\text{--}27)\ Ca(7\text{--}17)} \quad pH = 7.3\text{--}8.1.$$

At depths of 70–250 m, mineralization increases (up to a maximum 6.9 g/L) and the chemical composition of the groundwater changes:

$$S = 2.0\text{--}6.9 \quad \frac{\begin{array}{c} SO_4(46\text{--}85)\ Cl(7\text{--}51) \\ HCO_3(8\text{--}39) \end{array}}{Na(37\text{--}80)\ Ca(11\text{--}35)\ Mg(9\text{--}28)} \quad pH = 7.1\text{--}7.8.$$

The initial chemical composition of groundwater in this zone was formed, most likely, under the gypsum dissolution, and later calcium was partially exchanged with sodium from sediments.

At depths of 250–400 m, there is a noticeable decrease of salinity and the next change in the chemical composition of groundwater:

$$S = 1.8\text{--}4 \quad \frac{\begin{array}{c} Cl(34\text{--}71)\ SO_4(18\text{--}32) \\ HCO_3(2\text{--}7) \end{array}}{Ca(45\text{--}74)\ Mg(6\text{--}21)\ Na(12\text{--}34)} \quad pH = 7.5\text{--}8.5.$$

Thus, a specific feature of this region is vertical chemical inversion (Figure 4), which is mainly caused by variations in the SO_4^{2-}, Ca^{2+} and Na^+ content.

River valleys are the most probable areas for the upward discharge of brackish deep-water. Such anomalies are simultaneously observed in the groundwater salinity, the hydraulic head, and the uranium isotopic composition (Figures 5 and 6). Hereinafter, the term "anomalies of the uranium isotopic composition" will mean the ratio $^{234}U/^{238}U > 7.8$, i.e., the top quantile of the total samples. Watersheds with low mineralization of groundwater and a regular hydraulic head are areas of modern recharge. In the areas with anomalies of the isotopic composition of uranium, the groundwater also has relatively low temperatures (Figure 7).

Anomalies in the $^{234}U/^{238}U$ ratios were found in groundwater with different salinity, S = 0.4–2.4 g/L, which is a result of mixing when the brackish deep-water moves upward to the modern surface due to excess of the hydraulic head (Figure 6). The mixing of groundwater significantly complicates the interpretation of the chemical and $^{234}U/^{238}U$ data. Therefore, the stable isotope composition of the groundwater ($\delta^{18}O$ and δ^2H) was determined (Figure 8).
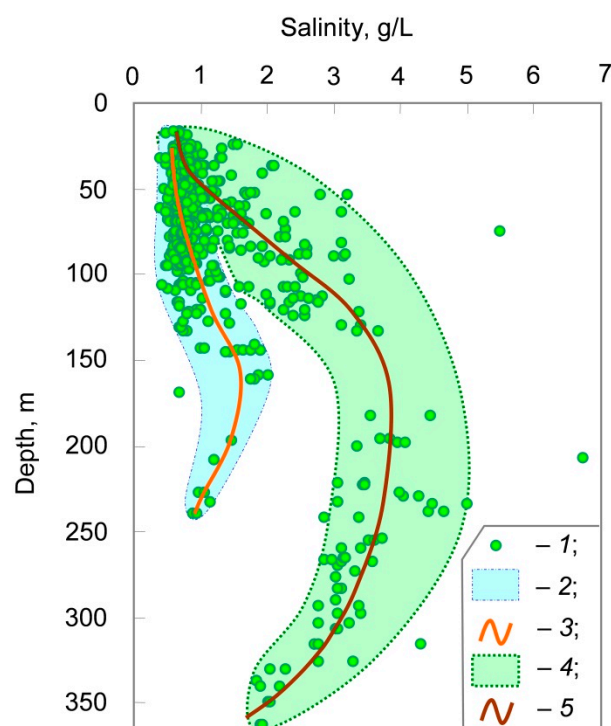
Figure 4. Vertical chemical zonation of groundwater in the Pre-Volga region (results of sampling of 839 boreholes in 1990–2005): *1*—individual analysis ("Depth" on the ordinate is mean a middle depth of the borehole screen); *2,3*—field of groundwater mineralization of the Mesozoic structural stage and approximation line; *4,5*—field of groundwater salinity of the Upper Permian structural stage and the approximation line.
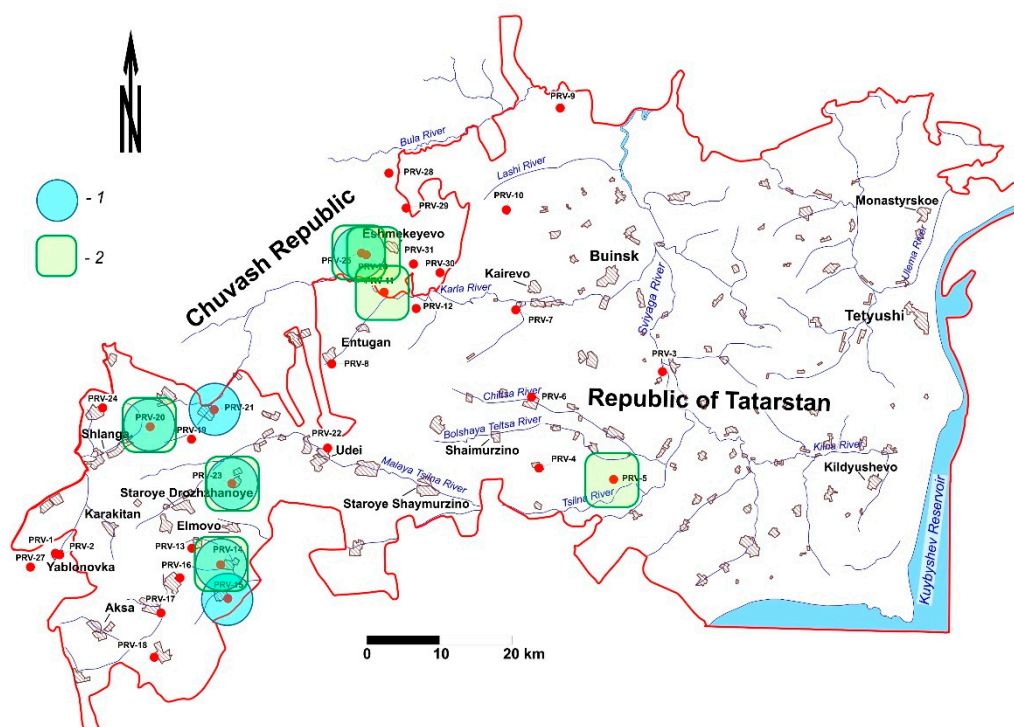

Figure 5. Areas with anomalies in the uranium isotopic composition and hydraulic head: *1*—anomalies of the uranium-234 content ($^{234}U/^{238}U > 7.8$); *2*—points where the hydraulic head, calculated taking into account the temperature and water salinity, deviates from the regional trend (Figure 6).
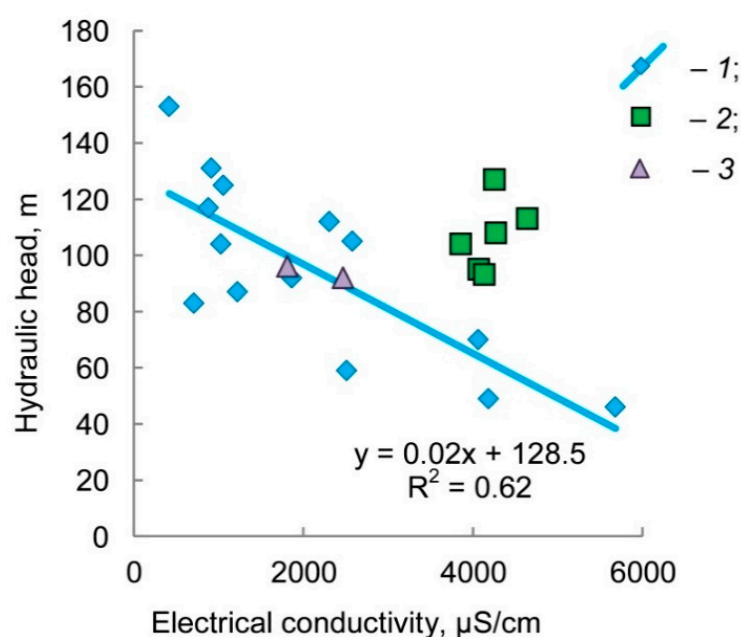
Figure 6. Relationship between the electrical conductivity and the hydraulic heads of groundwater in the Pre-Volga region: *1*—points where the hydraulic head does not deviate from the regional trend (equation of the approximation line is on the diagram); *2*—points where anomalies of the hydraulic heads and the uranium isotopic composition (^{234}U/^{238}U > 7.8) were found; and *3*—outliers (explanation in the text below).
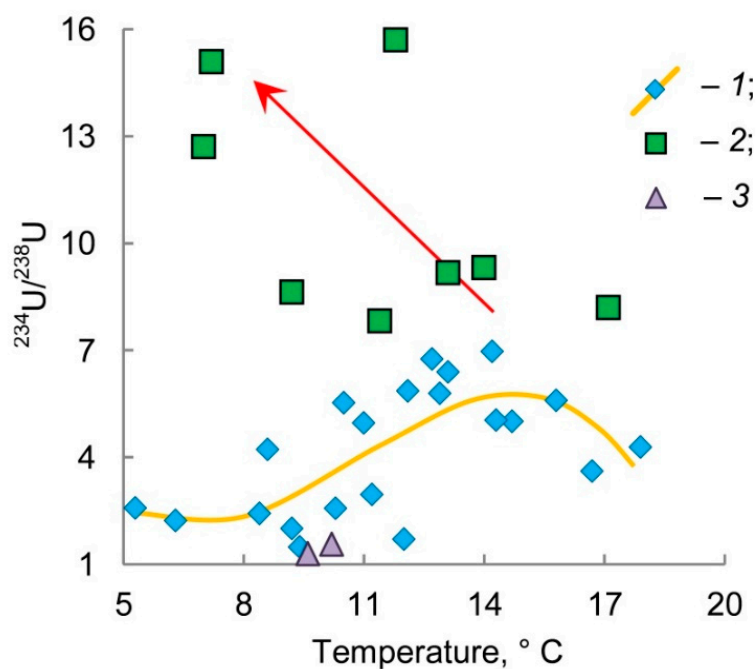

Figure 7. Relationship between the water temperature and the isotopic composition of uranium in groundwater of the Pre-Volga region: *1*—points without anomalies (^{234}U/^{238}U < 7.8, on diagram shown as the approximation curve); *2*—points with anomalies of the uranium isotopic composition (arrow is a general trend for these cases); and *3*—outliers.
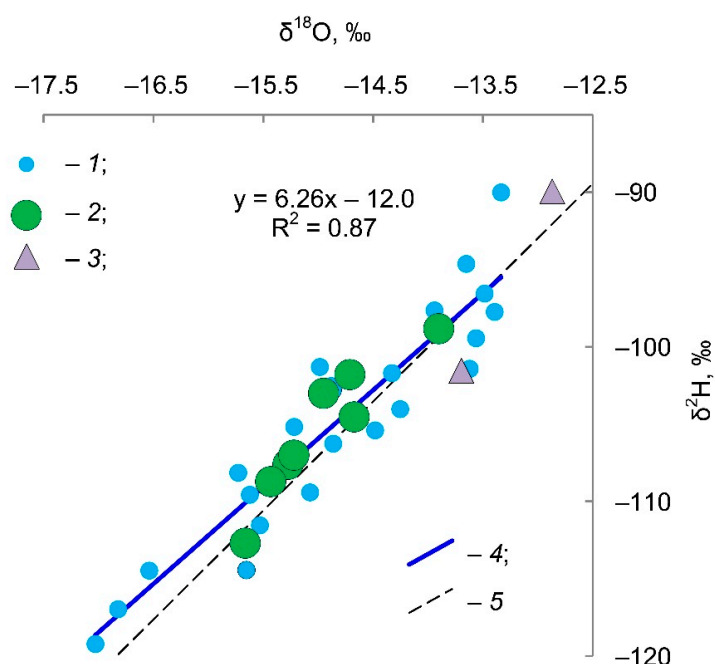
Figure 8. The stable isotopes composition of groundwater in the Pre-Volga region: *1*—points without anomalies of the isotopic composition of uranium (^{234}U/^{238}U < 7.8); *2*—points with anomalies of the uranium isotopic composition; *3*—outliers; *4*—the linear approximation of the total data (equation in the diagram); and *5*—local meteoric water line.

Comparison of the ^{234}U/^{238}U ratios and the stable isotope compositions of groundwater in the Pre-Volga region shows the three-component mixture of the groundwater (Figure 9).

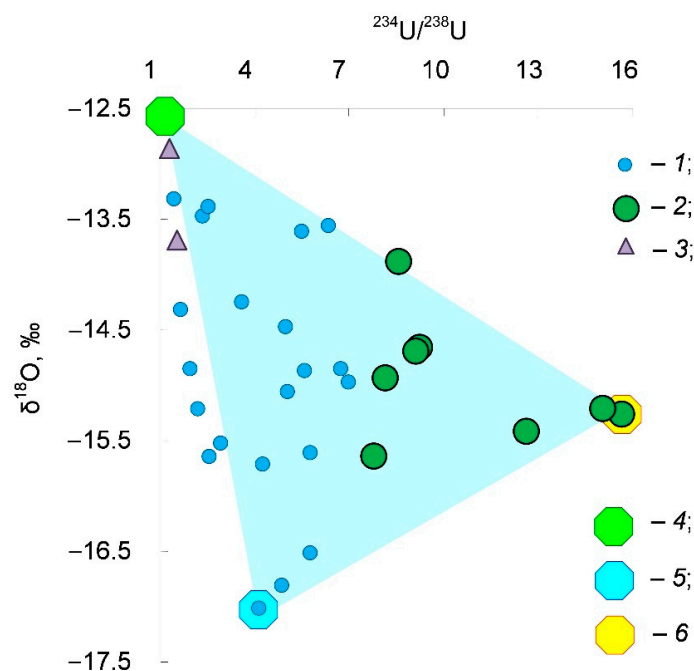**Figure 9.** Comparison of the isotopic composition of uranium and oxygen-18 content in groundwater of the Pre-Volga region: *1*—points without anomalies of the isotopic composition of uranium (^{234}U/^{238}U < 7.8); *2*—points with anomalies of the uranium isotopic composition; *3*—outliers; and *4, 5,* and *6*—mixing end-members "modern water", "postglacial water" and "glacial meltwater", respectively.

1. Modern and/or young (Holocene age) recharge water with salinity S < 0.5 g/L. It has the least depletion in the isotopic composition of hydrogen and oxygen $\delta^{18}O \rightarrow -12.9$ ‰ and $\delta^2H \rightarrow -90$ ‰, which is close to the modern precipitation of the region, and practically the equilibrium isotope composition of uranium $^{234}U/^{238}U \rightarrow 1$.
2. Water of the late and/or postglacial genesis. It has a slight increase in salinity S ≈ 0.5–1.5 g/L, the isotopically lightest composition $\delta^{18}O \rightarrow -17.0$ ‰ and $\delta^2H \rightarrow -119$ ‰ (maybe water of a proglacial lake?), and a small excess of uranium-234 $^{234}U/^{238}U \approx 4$.
3. The glacial meltwater formed due to the permafrost thawing. It is the brackish water S → 3 g/L (for these 33 samples under consideration). This water has the intermediate composition of the stable isotopes $\delta^{18}O \approx -15.0$ ‰ and $\delta^2H \approx -110$ ‰ (ice in permafrost, most likely, formed from mixture water of the Valdai cryochron and the previous interstadial), and maximum disequilibrium in uranium $^{234}U/^{238}U \rightarrow 15.7$.

Theoretically, as a result of the cryogenic metamorphization during permafrost formation, the glacial meltwater should have:

*   reduced mineralization, as salts must be lost in the freezing process;
*   an isotope composition of hydrogen and oxygen with less depletion than the recharge water (points must have a shift to the right from the meteoric line on the δ2H vs. δ18O diagram).

The salinity of the glacial meltwater in the Pre-Volga region varies within a wide range S = 0.4–2.4 g/L. This could result from the presence of evaporites in the water-bearing sediments and the increased solubility of the iron and manganese sulfates (melanterite and jarosite) at near-zero temperature. During the Valdai cryochron, the temperature of the geological section transited through zero many times, which led to the predominance of sulfates in the anionic composition.

An explanation should be given about two data points designated in all the above diagrams by term "outliers". It can clearly be seen from stable isotopes and from the $^{234}U/^{238}U$ ratio (Figure 8) that it is modern groundwater. The chemical composition of groundwater at these two points does not fit the general picture (see excess of Ni on Figure 10) due to the local geochemical specialization of water-bearing rocks.
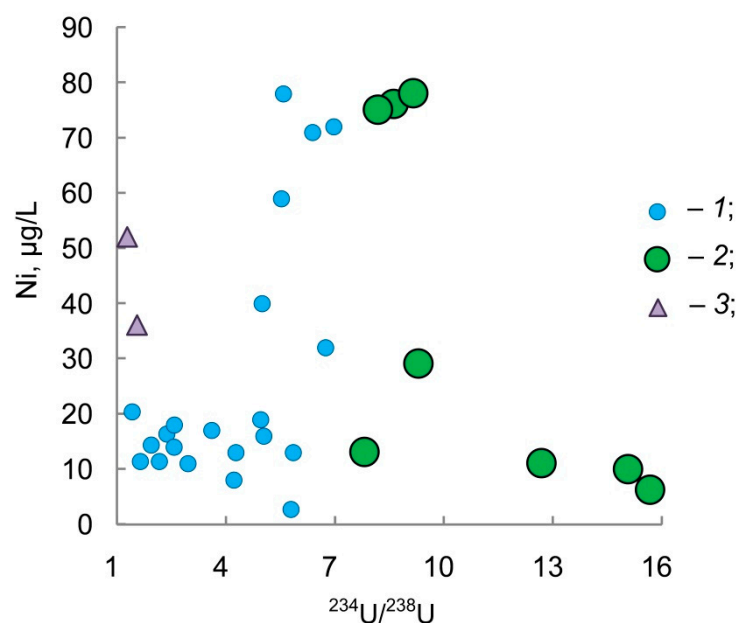

Figure 10. Relationship between the isotopic composition of uranium and nickel content in groundwater of the Pre-Volga region: *1*—points without anomalies of the isotopic composition of uranium ($^{234}U/^{238}U$ < 7.8); *2*—points of anomalies of the uranium isotopic composition; and *3*—outliers.

5. Conclusions

The proxy markers of the existence of permafrost were found in the isotope and chemical compositions of groundwater for the Pre-Volga region. Joint analysis of the groundwater chemistry, the isotopic composition of uranium (^{234}U/^{238}U by activity), and the stable isotopes (contents of deuterium and oxygen-18) made it possible to define the contribution of the mixing of three end-members:

- Modern and/or young recharge water of the infiltration origin has the lowest salinity S < 500 mg/L, the heaviest stable isotope composition δ^{18}O → −12.9 ‰ and δ^{2}H → −90 ‰ close to modern precipitation, and practically equilibrium uranium ^{234}U/^{238}U → 1;
- Late and/or postglacial water, which has a slight increase in mineralization S ≈ 0.5–1.5 g/L, the lightest isotopic composition δ^{18}O → −17.0 ‰ and δ^{2}H → −119 ‰, and a small excess of uranium-234 ^{234}U/^{238}U ≈ 4;
- Glacial meltwater (groundwater formed from thawing permafrost) has increased salinity S → 3 g/L, an intermediate composition of the stable isotopes δ^{18}O ≈ −15.0 ‰ and δ^{2}H ≈ −110 ‰, and maximum excess of uranium-234 ^{234}U/^{238}U → 15.7.

None of the end-members were found in a pure form, except the modern infiltration water, which is due to the impossibility of carrying out special drilling operations to test the geological section within this study. However, this typing of groundwater is in accordance with a general trend of the climate evolution on the studied area in the Late Pleistocene and Holocene. Using isotope tracers makes it possible to eliminate the difficulties caused by the variety of conditions of chemical interaction in the water-rock system in identifying glacial meltwater.

Analysis of the chemical data indicates the existence of geochemical specialization in certain locations of the studied area, possibly associated with explosive tectonics.

In the next stage, a detailed sampling at the sites of the clearest manifestation of the glacial meltwater and carrying out monitoring observations are planned.

Author Contributions: All authors contributed to the study conception and design. Conceptualization, validation, and writing—original draft preparation are performed by E.Y. and I.T. Methodology was performed by E.Y. and I.T., S.I., S.Z. and N.I. Formal analysis and investigation were performed by I.T., E.Y., S.I., S.Z. and N.I. Writing—review and editing were performed by E.Y. and I.T. Funding acquisition were performed by E.Y and I.T. Project administration and resources were performed by E.Y. and I.T. Supervision and visualization were performed by E.Y. and I.T. All authors have read and agreed to the published version of the manuscript.

Institutional Review Board Statement: Not applicable.

Informed Consent Statement: Not applicable.

Data Availability Statement: The datasets presented in this study can be obtained upon request to the corresponding author.

Conflicts of Interest: The authors declare no conflict of interest.

Appendix A

Table A1. Groundwater sampling points in the Pre-Volga region.

Sample ID	Sites of Groundwater Collection	Coordinates		Geological Age
		Latitude	Longitude	
PRV-1	Yablonovka Village	54.67640	47.33320	K_2
PRV-2	Yablonovka Village	54.67738	47.33272	K_2
PRV-3	Nemchinovka Village	54.87359	48.38206	P_2t
PRV-4	Chuvash Kischak Village	54.77169	48.16469	P_2kz
PRV-5	Yaskul Village	54.76633	48.30734	P_2kz
PRV-6	Old Tinchali Village	54.84544	48.15256	P_2kz
PRV-7	Mullanur Vakhitov Village	54.93067	48.12241	P_2t
PRV-8	Volny Stan Village	54.87190	47.80623	P_2kz
PRV-9	Kamennyi Brod Village	55.14796	48.17735	P_2t
PRV-10	Tatar Belovozhka Village	55.03437	48.10233	P_2t
PRV-11	Malye Shikhardans Village	54.95153	47.85416	P_2t
PRV-12	Embulatovo Village	54.93251	47.95070	P_2t
PRV-13	Staroe Ilmovo Village	54.68475	47.57681	P_2kz
PRV-14	Novoe Ilmovo Village	54.67081	47.61837	P_2kz
PRV-15	Novie Chukaly Village	54.63715	47.63321	P_2kz
PRV-16	Starie Chukaly Village	54.65622	47.55037	P_2kz
PRV-17	Bolshaya Aksa Village	54.63486	47.50940	P_2kz
PRV-18	Gorodishe Village	54.57689	47.51139	P_2kz
PRV-19	Novye Ishli Village	54.79223	47.56261	P_2kz
PRV-20	Staryie Ishli Village	54.80350	47.49523	P_2kz
PRV-21	Novye Kakerly Village	54.82065	47.60283	P_2kz
PRV-22	Malyi Ubei Village	54.78862	47.79419	J_2k-km
PRV-23	Alyoshkin Saplyk Village	54.74966	47.63657	P_2kz
PRV-24	Shlanga Village	54.81568	47.40597	P_2kz
PRV-25	Kyzyl-Chishma Village	54.99799	47.80966	P_2t
PRV-26	Kyzyl-Chishma Village	54.99772	47.81442	P_2t
PRV-26/1	Kyzyl-Chishma Village	54.99750	47.81577	Q
PRV-26/2	Kyzyl-Chishma Village	54.99178	47.79538	Q
PRV-27	Rifulka tract	54.66155	47.29987	K_2
PRV-28	Yantikovo Village	55.09047	47.86835	P_2t
PRV-29	Ishmurzino-Surinsk Village	55.05441	47.89444	P_2t
PRV-30	Yamanchurino Village	54.97296	47.96838	P_2t
PRV-31	Shemalakovo Village	54.97709	47.90161	P_2t

References

1. Gerasimov, I.P.; Markov, K.K. Ice Age on the USSR. In *Proceedings of the Institute of Geography*; Academy of Sciences of the USSR: Moscow, Russia, 1939; p. 462.
2. Velichko, A.A. *Natural process in the Pleistocene*; Nauka Publishers: Moscow, Russia, 1973; p. 256. (In Russian)
3. Butakov, G.P. *Pleistocene peglacial in the east of the Russian Plain*; Kazan State University, Kazan Publishing House: Kazan, Russia, 1986; p. 144.
4. Hubberten, H.W.; Andreev, A.; Astakhov, V.I.; Demidov, I.; Dowdeswell, J.A.; Henriksen, M.; Hjort, C.; Houmark-Nielsen, M.; Jakobsson, M.; Kuzmina, S.; et al. The periglacial climate and environment in northern Eurasia during the Last Glaciation. *Quat. Sci. Rev.* **2004**, *23*, 1333–1357. [CrossRef]
5. Houmark-Nielsen, M.; Demidov, I.; Funder, S.; Grøsfjeld, K.; Kjær, K.H.; Larsen, E.; Lavrova, N.; Lyså, A.; Nielsen, J.K. Early and Middle Valdaian glaciations, ice-dammed lakes and periglacial interstadials in northwest Russia: New evidence from the Pyoza River area. *Glob. Planet. Chang.* **2001**, *31*, 215–237. [CrossRef]
6. Kalm, V.; Gorlach, A. Impact of bedrock surface topography on spatial distribution of Quaternary sediments and on the flow pattern of late Weichselian glaciers on the East European Craton (Russian Plain). *Geomorphology* **2014**, *207*, 1–9. [CrossRef]

7. Lasberg, K.; Kalm, V.; Kihno, K. Ice-free interval corresponding to marine isotope stages 4 and 3 at the last glacial maximum position at Kileshino, Valdaj upland, Russia. *Estonian J. Earth Sci.* **2014**, *63*, 88–96. [CrossRef]
8. Velichko, A.A.; Faustova, M.A.; Gribchenko, Y.N.; Pisareva, V.V.; Sudakova, N.G. Glaciations of the East European Plain—distribution and chronology. In *Developments in Quaternary Sciences*; Ehlers, J., Gibbard, P.L., Eds.; Elsevier: Amsterdam, The Nederland, 2004; pp. 337–354. [CrossRef]
9. Velichko, A.A.; Morozova, T.D.; Nechaev, V.P.; Rutter, N.W.; Dlusskii, K.G.; Little, E.C.; Catto, N.R.; Semenov, V.V.; Evans, M.E. Loess/paleosol/cryogenic formation and structure near the northern limit of loess deposition, East European Plain, Russia. *Quat. Int.* **2006**, *152–153*, 14–30. [CrossRef]
10. Velichko, A.A.; Faustova, M.A.; Pisareva, V.V.; Gribchenko, Y.U.N.; Sudakova, N.G.; Lavrentiev, N.V. Glaciations of the east European plain—Distribution and chronology. *Dev. Quat. Sci.* **2011**, *15*, 337–359. [CrossRef]
11. Svendsen, J.I.; Alexanderson, H.; Astakhov, V.I.; Demidov, I.; Dowdeswell, J.A.; Funder, S.; Gataullin, V.; Henriksen, M.; Hjort, C.; Houmark-Nielsen, M.; et al. Late Quaternary ice sheet history of northern Eurasia. *Quat. Sci. Rev.* **2004**, *23*, 11–13. [CrossRef]
12. Lisiecki, L.E.; Raymo, M.E. A Pliocene-Pleistocene stack of 57 globally distributed benthic δ^{18}O records. *Paleoceanogr. Paleoclimatol.* **2005**, *20*, 1–17. [CrossRef]
13. Velichko, A.A.; Zelikson, E.M. Landscape, climate and mammoth food resources in the East European Plain during the Late Paleolithic epoch. *Quat. Int.* **2005**, *126–128*, 137–151. [CrossRef]
14. Linge, H.; Larsen, E.; Kjær, K.H.; Demidov, I.; Brook, E.J.; Raisbeck, G.M.; Yiou, F. Cosmogenic ^{10}Be exposure age dating across Early to Late Weichselian ice-marginal zones in northwestern Russia. *Boreas* **2006**, *35*, 576–586. [CrossRef]
15. Ehlers, J.; Astakhov, V.; Gibbard, P.L.; Mangerud, J.; Svendsen, J.I. Glaciations | Late Pleistocene Glaciations in Europe. In *Encyclopedia of Quaternary Science*; Elias, S.A., Ed.; Elsevier: Amsterdam, The Netherlands; pp. 1085–1095. [CrossRef]
16. Sycheva, S.; Sedov, S. Paleopedogenesis during the Mikulino interglacial (MIS 5e) in the East-European plain: Buried toposequence of the key-section «Alexandrov quarry». *Boletín de la Sociedad Geológica Mexicana* **2012**, *64*, 189–197. [CrossRef]
17. Yanina, T.A. Correlation of the Late Pleistocene paleogeographical events of the Caspian Sea and Russian Plain. *Quat. Int.* **2012**, *271*, 120–129. [CrossRef]
18. Helmens, K.F. The last interglacial-glacial cycle (MIS 5-2) re-examined based on long proxy records from central and northern Europe. *Quat. Sci. Rev.* **2014**, *86*, 115–123. [CrossRef]
19. Hughes, A.L.C.; Gyllencreutz, R.; Lohne, Ø.S.; Mangerud, J.; Svendsen, J.I. The last Eurasian ice sheets—a chronological database and time-slice reconstruction, DATED-1. *Boreas* **2016**, *45*, 1–45. [CrossRef]
20. Astakhov, V.; Shkatova, V.; Zastrozhnov, A.; Chuyko, M. Glaciomorphological Map of the Russian Federation. *Quat. Int.* **2016**, *420*, 4–14. [CrossRef]
21. Andreicheva, L.N.; Ponomarev, D.V. Litho- and biostratigraphy of the middle neopleistocene of the European northeast of Russia. *Stratigr. Geol. Correl.* **2018**, *26*, 584–597. [CrossRef]
22. Zastrozhnov, A.; Danukalova, G.; Shick, S.; Kolfshoten, T. State of stratigraphic knowledge of Quaternary deposits in European Russia: Unresolved issues and challenges for further research. *Quat. Int.* **2018**, *478*, 4–26. [CrossRef]
23. Sycheva, S.; Pushkina, P.; Khokhlova, O.; Ukrainsky, P. Interrelations of the Bryansk paleosol (end of MIS 3) with the Holocene surface soils in micro-depressions of the central forest-steppe within the Russian upland. *Catena* **2019**, *172*, 619–633. [CrossRef]
24. Ponomarev, D.; Andreicheva, L. Middle-upper quaternary stratigraphy in the northeast of European Russia inferred from rodent record and lithology of tills. *Quat. Int.* **2019**, *534*, 60–72. [CrossRef]
25. Astakhov, V.I. *The Northern Pleistocene of Russia*; Cambridge Scholars Publishing; Lady Stephenson Library: Newcastle upon Tyne, UK, 2020; p. 610.
26. Makeev, A.; Rusakov, A.; Khokhlova, O.; Kust, P.; Mikhaylova, D.; Aseyeva, E.; Kurbanova, F.; Rusakova, E.; Mihailov, E. Dataset on spatial variability of soil properties: Tokhmeyevo archaeological site of the bronze age, Chuvashia (southern fringe of the forest zone, the Russian plain). *Data Brief* **2020**, *33*, 106489. [CrossRef]
27. Andreev, A.A.; Gromig, R.; Wagner, B.; Wennrich, V.; Melles, M.; Shumilovskikh, L.S.; Savelieva, L.A.; Fedorov, G.B.; Ludikova, A.; Brill, D. Environmental conditions in northwestern Russia during MIS 5 inferred from the pollen stratigraphy in a sediment core from Lake Ladoga. *Boreas* **2019**, *48*, 377–386. [CrossRef]
28. Bolikhovskaya, N.S.; Molodkov, A.N. East European loess–palaeosol sequences: Palynology, stratigraphy and correlation. *Quat. Int.* **2006**, *149*, 24–36. [CrossRef]
29. *Atlas of the Republic of Tatarstan (2005) Cartographic Edition*; Cartography: Moscow, Russia, 2005; 215p. (In Russian)
30. Markova, A.; Kolfschoten, V.T.; Puzachenko, A.Y. *Evolution of the European Ecosystems during Pleistocene–Holocene Transition (24–8 kyr BP)*; GEOS: Moscow, Russia, 2008; p. 277.
31. Markova, A.K.; Simakova, A.N.; Puzachenko, A.Y. Ecosystems of Eastern Europe at the time of maximum cooling of the Valdai glaciation (24–18 kyr BP) inferred from data on plant communities and mammal assemblages. *Quat. Int.* **2009**, *201*, 53–59. [CrossRef]
32. Markova, A.K.; Puzachenko, A.Y. European small mammal faunas during Dnieper (Saale) glaciation and transition to the Mikulino (Eem) interglacial. *Quat. Int.* **2020**. [CrossRef]
33. Novenko, E.Y. Late Valdai pollen flora from loess sediments in the central East-European Plain. Paleoenvironmental reconstruction. *Quat. Int.* **2006**, *152–153*, 146–152. [CrossRef]

34. Novenko, E.Y.; Olchev, A.V. Early Holocene vegetation and climate dynamics in the central part of the East European Plain (Russia). *Quat. Int.* **2015**, *388*, 12–22. [CrossRef]

35. Puzachenko, A.Y.; Markova, A.K. Diversity dynamics of large- and medium-sized mammals in the Late Pleistocene and the Holocene on the East European Plain: Systems approach. *Quat. Int.* **2016**, *420*, 391–401. [CrossRef]

36. Simakova, A.N. The vegetation of the Russian Plain during the second part of the Late Pleistocene (33–18 ka). *Quat. Int.* **2006**, *149*, 110–114. [CrossRef]

37. Little, E.C.; Lian, O.B.; Velichko, A.A.; Morozova, T.D.; Nechaev, V.P.; Dlussky, K.G.; Rutter, N.W. Quaternary stratigraphy and optical dating of loess from the east European Plain (Russia). *Quat. Sci. Rev.* **2002**, *21*, 1745–1762. [CrossRef]

38. Panin, P.G.; Timireva, S.N.; Morozova, T.D.; Kononov, Y.M.; Velichko, A.A. Morphology and micromorphology of the loess-paleosol sequences in the south of the East European plain (MIS 1–MIS 17). *Catena* **2018**, *168*, 79–101. [CrossRef]

39. Panin, A.V.; Astakhov, V.I.; Lotsari, E.; Komatsu, G.; Lang, J.; Winsemann, J. Middle and Late Quaternary glacial lake-outburst floods, drainage diversions and reorganization of fluvial systems in northwestern Eurasia. *Earth Sci. Rev.* **2020**, *201*, 103069. [CrossRef]

40. Sidorchuk, A.Y.; Panin, A.V.; Borisova, O.K. Morphology of river channels and surface runoff in the Volga River basin (East European Plain) during the Late Glacial period. *Geomorphology* **2009**, *113*, 137–157. [CrossRef]

41. Velichko, A.A. (Ed.) Paleoclimates and paleolandscapes of the extratropical space of the Northern Hemisphere. In *Late Pleistocene–Holocene*; GEOS: Moscow, Russia, 2009; p. 120. (In Russian)

42. Rusakov, A.; Nikonov, A.; Savelieva, L.; Simakova, A.; Sedov, S.; Maksimov, F.; Kuznetsov, V.; Savenko, V.; Starikova, A.; Korkka, M.; et al. Landscape evolution in the periglacial zone of Eastern Europe since MIS5: Proxies from paleosols and sediments of the Cheremoshnik key site (Upper Volga, Russia). *Quat. Int.* **2015**, *365*, 26–41. [CrossRef]

43. Rusakov, A.; Sedov, S.; Sheinkman, V.; Dobrynin, D.; Zinovyev, E.; Trofimova, S.; Maksimov, F.; Kuznetsov, V.; Korkka, M.; Levchenko, S. Late Pleistocene paleosols in the extra-glacial regions of Northwestern Eurasia: Pedogenesis, post-pedogenic transformation, paleoenvironmental inferences. *Quat. Int.* **2019**, *501*, 174–192. [CrossRef]

44. Simonova, J.; Rusakov, A.; Ryumin, A.; Mirin, D.; Lemeshko, N.; Popov, A.; Rusakova, E. The response of salt-affected hydromorphic soils of the Nero Lake basin to the recent climate change within the Upper Volga Region, Russia. *Soil Tillage Res.* **2021**, *207*, 104871. [CrossRef]

45. Sidorchuk, A.; Borisova, O.; Panin, A. Fluvial response to the Late Valdai/Holocene environmental change on the East European Plain. *Glob. Planet. Chang.* **2001**, *28*, 303–318. [CrossRef]

46. Zaretskaya, N.; Panin, A.; Molod'kov, A.; Trofimova, S.; Simakova, A.; Baranov, D. Pleistocene stratigraphy of the Vychegda River basin, European North-East. *Quat. Int.* **2020**, *546*, 185–195. [CrossRef]

47. Zaretskaya, N.E.; Panin, A.V.; Karpukhina, N.V. The SIS limits and related proglacial events in the Severnaya Dvina basin, northwestern Russia: Review and new data. *Bull. Geol. Soc. Finl.* **2018**, *90*, 301–313. [CrossRef]

48. Cohen, K.M.; Gibbard, P.L. Global chronostratigraphical correlation table for the last 2.7 million years, version 2019 QI-500. *Quat. Int.* **2019**, *500*, 20–31. [CrossRef]

49. Jones, M.D.; Dee, S.; Anderson, L.; Baker, A.; Bowen, G.; Noone, D.C. Water isotope systematics: Improving our palaeoclimate interpretations. *Quaternary Sci. Rev.* **2016**, *131*, 243–249. [CrossRef]

50. Miller, G.H.; Brigham-Grette, J.; Alley, R.B.; Anderson, L.; Bauch, H.A.; Douglas, M.S.V.; Edwards, M.E.; Elias, S.A.; Finney, B.P.; Fitzpatrick, J.J.; et al. Temperature and precipitation history of the Arctic. *Quaternary Sci. Rev.* **2010**, *29*, 1679–1715. [CrossRef]

51. Négrel, P.; Petelet-Giraud, E. Isotopes in groundwater as indicators of climate changes. *Trends Analytical Chem.* **2011**, *30*, 1279–1290. [CrossRef]

52. Paillard, D. Quaternary glaciations: From observations to theories. *Quat. Sci. Rev.* **2015**, *107*, 11–24. [CrossRef]

53. Ferronsky, V.I.; Vlasova, L.S.; Esikov, A.D.; Zorin, L.V.; Borisova, Z.K.; Polyakov, V.A.; Seletsky, Y.B.; Punning, Y.-M.K.; Vaikmäe, R.A. Variations in the isotopic composition of groundwater, atmospheric precipitation and organic matter in alluvial sediments due to climate fluctuations. *Water Res.* **1982**, *5*, 6–23.

54. Suksi, U.J.; Rasilainen, K.; Ruskeeniemi, T.; Marcos, N.; Hellmuth, K.H. Natural U occurrences as a palaeo-hydrogeological indicator—observations from the Palmottu natural analogue site, Finland. In *Uranium in the Aquatic Environment*; Merkel, B.J., Planer-Friedrich, B., Wolkersdorfer, C., Eds.; Springer: Berlin/Heidelberg, Germany, 2002. [CrossRef]

55. Francke, A.; Dosseto, A.; Just, J.; Wagner, B.; Jones, B.G. Assessment of the controls on (234U/238U) activity ratios recorded in detrital lacustrine sediments. *Chem. Geol.* **2020**, *550*, 119698. [CrossRef]

56. Kayzar, T.M.; Villa, A.C.; Lobaugh, M.L.; Gaffney, A.M.; Williams, R.W. Investigating uranium distribution in surface sediments and waters: A case study of contamination from the Juniper Uranium Mine, Stanislaus National Forest, CA. *J. Environ. Radioactivity* **2014**, *136*, 85–97. [CrossRef]

57. Tokarev, I.V.; Bubnov, Y.P.; Kharkhordin, I.L. Conditions for the formation of resources and the quality of groundwater in the southwest of the Republic of Tatarstan according to geochemical and isotope data. In *Materials of the International Conference "The Future of Hydrogeology: Current Trends and Prospects"*; St. Petersburg State University: St. Petersburg, Russia, 2008; pp. 196–208.

58. Tokarev, I.V.; Zubkov, A.A.; Rumynin, V.G.; Pozdnyakov, S.P.; Polyakov, V.A.; Kuznetsov, V.Y. Assessment of the long-term safety of radioactive waste disposal: 1. Paleoreconstruction of groundwater formation conditions. *Water Res.* **2009**, *36*, 206–213. [CrossRef]

59. Tokarev, I.V.; Zubkov, A.A.; Rumynin, V.G.; Pozdnyakov, S.P. Assessment of the long-term safety of radioactive waste disposal: 2. Isotopic study of water exchange in a multilayer system. *Water Res.* **2009**, *36*, 345–356. [CrossRef]

60. Tokarev, I.V.; Kipfer, R.; Tomonaga, Y.; Brennwald, M.S.; Vereschagina, E.A. Comparison of ^{4}He and ^{14}C dating, noble-gas temperatures and stable isotope (d^{2}H, d^{18}O) data for groundwater in stratified aquifers (Tomsk-7, S.E. Siberia). *Mineral. Mag.* **2011**, *75*, 2018. [CrossRef]

61. Manakov, A.V. *Kuibyshev Reservoir*; Nauka Publishers: Leningrad, Russia, 1983; p. 214. (In Russian)

62. Sycheva, S.A. Paleo-permafrost events in the periglacial area of the Central Russian Upland at the end of the Middle and Late Pleistocene. *Earth's Cryosphere* **2012**, *16*, 45–56. [CrossRef]

63. *Geology of the Republic of Tatarstan*; Kazan State University: Kazan, Russia, 2007; p. 74. (In Russian)